# Confined multiple impinging slot jets without crossflow effects

**N. R. Saad*, S. Polat and W. J. M. Douglas**
Department of Chemical Engineering and Pulp and Paper Research Centre, McGill University, Montreal, Canada

Transport data for single impinging jets are frequently used in the design of equipment that involves multiple impinging jets. Geometric and flow conditions at which jets in a multiple impinging jet system no longer behave as independent single jets are not known. In the present study criteria are developed to make this distinction by comparing turbulence, mean flow, and heat transfer characteristics of a jet in an array of confined impinging slot jets with those of a single jet. Flow analysis showed that a flow cell, defined as volume contained by the impingement and confinement surfaces and the centerlines of adjacent inlet and exhaust ports, is characterized effectively with a single nondimensional ratio $S/H$, the ratio of the lateral and axial length of flow cell. The second nondimensional ratio necessary for complete geometric similarity of flow cells affects the pressure profiles to some extent only in the wall jet region. The critical $S/H$ ratio where jet-to-jet interactions become important is somewhere between 1–0.75. Heat transfer analysis showed that for flow cell ratio $S/H > 1.5$ a multiple jet system is effectively an assembly of single jets. For $S/H < 1.5$ interaction between adjacent jets increases heat transfer under the exhaust ports. For $S/H < 0.7$ this interaction causes a depression of stagnation heat transfer.

**Keywords:** single and multiple impinging jets; heat transfer; turbulence

## Introduction

High transfer rates relative to those for parallel flows and potential for fine control of local rates by adjusting the geometry and/or the local flow rate make impinging jets an attractive choice to cool, heat, or dry surfaces in a number of industrial applications. Cooling of electronic components, paper mill calendar rolls and turbine hardware, tempering of glass, anti-icing of aircraft wings and windshield surfaces, and drying of photographic films, textiles, and paper are examples of such industrial applications. Depending to some extent on the application, either round or slot jets may be used, either individually, in a single row, or in a multiple jet configuration.

The main motivation for the present work is the application of impinging jets to drying of paper. In this application, as large volumes of heating medium are required, economic considerations require recovery of the spent flow. Impinging jets must therefore be confined. Unfortunately, most laboratory investigations have been with unconfined jets. Without confinement, jets entrain ambient air, which affects heat transfer to an indeterminate extent depending on the relative values of nozzle exit, ambient, and impingement surface temperatures. Hence, heat transfer data obtained with unconfined jets cannot be used reliably for design of confined jet systems.

* Present address: Pratt and Whitney Canada Inc., Box 10, Longueuil, Quebec J4K 4X9, Canada.

Address reprint requests to Dr. Polat at her present address: The Procter & Gamble Company, Process Technology Department, Winton Hill Technical Center, 6250 Center Hill Road, Cincinnati, OH 45224, USA.

Received 5 August 1990; accepted 24 August 1991



Another design consideration for confined impinging jet systems is the exhaust flow arrangement for spent flow. If the removal of spent flow is not through exhaust ports located intermediate between the nozzles in the confinement surface, cross-flow of cumulative spent flow under the nozzle exit flow occurs. Cross-flow should be avoided whenever possible because of its adverse effect on impingement heat transfer.[1,2]

Transport processes under multiple impinging jets have received relatively little attention in spite of current and potential industrial significance. Also, there are distinct shortcomings among the few existing studies. Gardon and Akfirat[3] and Schuh and Pettersson[4] studied the heat transfer for unconfined multiple impinging jets. Such systems have little industrial relevance because lack of confinement of the jets into a closed system allows entrainment, and moreover, is inconsistent with the need to recover the spent flow. The only previous study of a confined multiple jet system is that of Martin,[5] who measured average mass transfer under multiple slot jets. Unfortunately, in that study the outflow did not occur through exhaust ports in the confinement surface but was constrained to exit only in the traverse direction through the open sides at the ends of the slot nozzles. As a consequence, the transport rate at the impingement surface was highly nonuniform in the direction of the nozzle length, an unacceptable characteristic in industrial applications such as drying of paper where uniformity in the traverse direction is essential.

Use of single jet data in the design of multiple jet systems is not uncommon. In a multiple jet system when the jets are spaced widely and therefore not interacting, this approximation is expected to be valid. However, in an opposite case where the jets are spaced closely and therefore highly interacting, special multiple jet data must be used in the design. None of the earlier

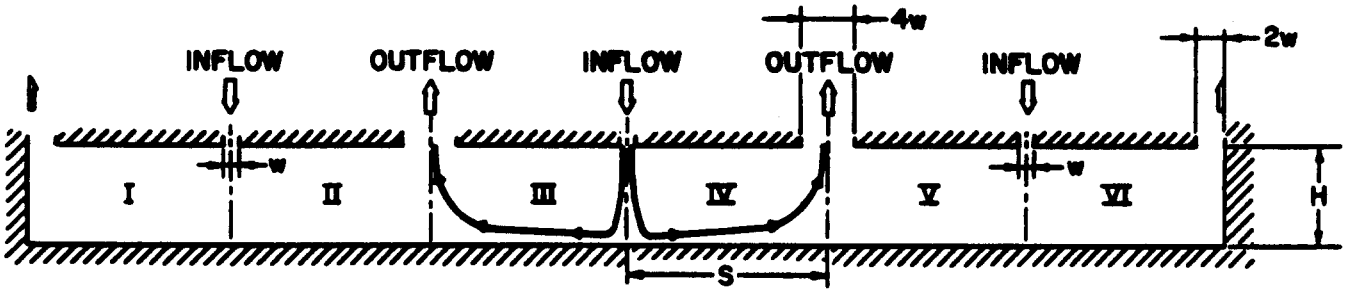


*Figure 1* Schematic diagram of test section

impinging jet studies have provided information as to geometric and flow conditions for which a multiple slot jet system deviates from that of an assembly of equivalent single jets. This then comprises the objective of the present work.

The present multiple jet system consists of three identical confined slot jets with symmetrical exhaust ports in the confinement surface (Figure 1). This type of arrangement avoids the forementioned shortcomings of the earlier studies on multiple jets. The middle jet of this three-jet system was shown to represent a jet in an array of impinging jets by measurements of static pressure and heat transfer profiles at the impingement surface. The geometric variables are nozzle width, $w$, spacing between the confinement and the impingement surfaces, $H$, and distance between the centerlines of adjacent inlet nozzles and exit ports, $S$. As the value of $S$ was fixed at 80 mm, both dimensionless centerline spacing, $S/w$, and fractional open area, $f = 2w/S$, are unique functions of nozzle width, which ranged from 6–32, and from 1.56–8.313, respectively. Use of $H$ values over the range 40–400 mm provided a wide range of dimensionless confinement-to-impingement surface spacing, $H/w$, from 4–24. The other geometric proportion defined for the first time in the present study to characterize multiple impinging jets is $S/H$, the ratio of width to depth of the basic flow cell, which recurs in the multiple impinging jet system. The present experimental apparatus comprised six flow cells, $6 > S/H > 0.375$. The basic flow parameter, Reynolds number at the nozzle exit, Re, ranged from about 3000–45,000.

## Flow characteristics of impinging jets

Flow field of an impinging jet comprises three characteristic regions, the free jet, stagnation flow, and wall jet. The nature of the free jet region depends greatly on the flow at the nozzle exit, which in turn is determined by the nozzle shape and dimensions. Depending on jet-to-impingement surface spacing, the free jet may also contain three characteristic regions, namely a potential core, developing, and developed flow regions. The potential core is that part of the free jet region where axial velocity remains effectively equal to nozzle exit velocity. High lateral gradients in axial mean velocity that exist directly under the nozzle walls constitute a region of correspondingly high generation of turbulence. Thus, the turbulence level in the free jet increases rapidly after discharge, including within the potential core region where mean velocity is unchanged from that at the nozzle exit.

In the stagnation flow region, static pressure first increases

## Notation

| | |
|---|---|
| $A_s$ | Free surface area of the heat flux sensor (for convection), mm |
| $f$ | Percent nozzle open area, = w/2S |
| $H$ | Nozzle-to-impingement surface spacing, mm |
| $h$ | Local heat transfer coefficient, W/m$^2$K |
| $k$ | Air thermal conductivity at the nozzle exit, W/mK |
| Nu | Local Nusselt number, hw/k |
| $Nu_e$ | Nusselt number under the exhaust port centerline |
| $Nu_0$ | Stagnation point Nusselt number |
| $P_s$ | Heat into the sensor, W |
| $\Delta P$ | Pressure relative to ambient, N/m$^2$ (Pa) |
| $\Delta P_j$ | Pressure difference across the nozzle jet, Pa |
| $\Delta P_0$ | Stagnation pressure relative to ambient, Pa |
| $Q_{cond}$ | Heat transfer by conduction, W |
| $Q_{conv}$ | Heat transfer by convection, W |
| $Q_{rad}$ | Heat transfer by radiation, W |
| $R_h$ | Resistance of the heating wire, ohm |
| $R_{lw}$ | Resistance of the lead wire, ohm |
| $R_P$ | Resistance of precision shunt, ohm |
| Re | Reynolds number at the nozzle exit, = $U_j^* w/\nu$ |
| $S$ | Jet centerline-to-exhaust centerline spacing, mm |
| $T_j$ | Jet temperature at the nozzle exit, °C |
| $T_s$ | Impingement surface temperature, °C |
| $U$ | Axial mean velocity, m/s |
| $U_j$ | Local mean velocity at the nozzle exit, m/s |
| $U_j^*$ | $U_j$ averaged across nozzle width, m/s |
| $U_{j0}$ | Nozzle exit centerline mean velocity, m/s |
| $U_0$ | Centerline mean velocity, m/s |
| $u$ | Axial instantaneous fluctuating velocity, m/s |
| $u'$ | Axial fluctuating velocity, $(u^2)^{0.5}$, m/s |
| $V_h$ | Voltage across the heating wire, volts |
| $V_P$ | Voltage across the precision resistance, volts |
| $w$ | Nozzle width, mm |
| $x$ | Lateral distance, mm |
| $y$ | Perpendicular distance from impingement surface, mm |
| $z$ | Axial distance from nozzle exit, mm |
| $\nu$ | Air kinematic viscosity, m$^2$/s |

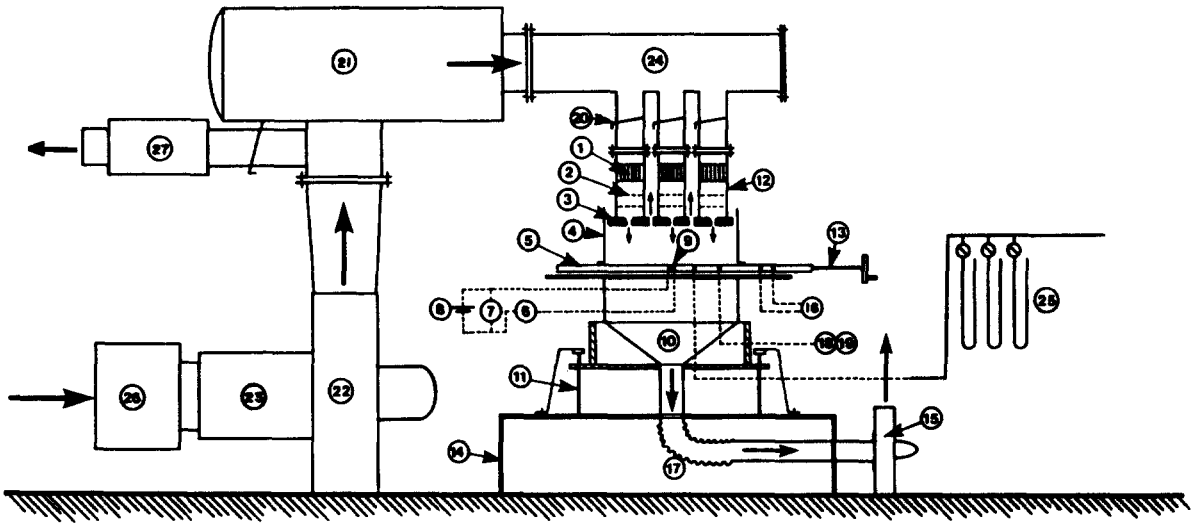

*Figure 2* Schematic diagram of the apparatus: 1, Honeycomb; 2, 100 mesh screen; 3, nozzle plate; 4, side wall; 5, impingement surface; 6, current measurement; 7, voltage measurement; 8, DC power supply; 9, heat flux sensor; 10, suction box; 11, impingement surface spacing adjustment; 12, plenum chamber; 13, screw for horizontal traversing; 14, level table; 15, blower to induce throughflow; 16, electrical heaters; 17, suction hose; 18, thermocouples; 19, temperature read-out; 20, butterfly valve; 21, main flow silencer; 22, air supply fan; 23, inlet air silencer; 24, header; 25, multimanometer panel; 26, air inlet filter; 27, bleed flow silencer

sharply, with the corresponding drop in axial velocity, then drops again as the flow accelerates along the impingement surface. The axial extent of the stagnation flow region is about 20–30 percent of the jet spacing, $H$.[9,14,17] The end of the stagnation flow in the lateral direction, defined as the location where the pressure gradient at the impingement surface becomes zero, occurs at about $0.35H$.[6–9]

Downstream of the impingement region is the wall jet region. For a confined jet, if the confinement and impingement surfaces are sufficiently long, the wall jet boundary layer grows to reach the confinement surface, thereby enclosing a recirculating bubble. In the case of an unconfined jet, entrainment of surrounding air affects the flow field and subsequently impingement surface transport characteristics to an undetermined amount. Thus, the use of results for unconfined jet systems in the design of confined jet systems may cause errors that exceed the expected uncertainty of the experimental data.

Flow field of multiple impinging jets contain an additional region to those described for a single impinging jet, i.e., the region where the deflected jets approach one another. Characteristics of this region, as expected, greatly depend on the type of outflow. For a system of three unconfined slot jets spaced at $16w$, Gardon and Akfirat[3] measured the static pressure at the impingement surface for jet spacings of $4w$ and $16w$ and Re = 5500. For the fixed internozzle spacing ($2S$) of $16w$, the narrow jet spacing, $4w$, resulted in a wall jet region four times larger than that for the wider jet spacing, $16w$. Static pressure profile of the middle jet in the former case differed from that of a single jet by large peaks only in a region where deflected jets approach one another. For the latter case the peaks were not as pronounced, but the pressure profile in general differed from that of a single jet, depressed in the stagnation flow region and elevated in the remainder of flow, indicating a greater jet-to-jet interaction. In another study, Romanenko and Davidzon[10] measured static pressure profiles under a similar unconfined jet system to that of Gardon and Akfirat for the combinations $H/w = 10$, $S/w = 12.5$ and $H/w = 20$, $S/w = 20.3$ and for a jet Reynolds number of about 9000. They obtained similar results to those of Gardon and Akfirat. Studies on the flow field of confined multiple impinging jet systems are very limited. The multiple slot jet system of Martin and Schlunder[18] suffered from three-dimensional effects as outflow was allowed in the traverse direction. This type of outflow is not suitable for paper drying as cross machine uniformity is an important specification. No study of flow for a multiple confined impinging slot jet system with symmetrical, two-dimensional (2-D) outflow has yet been published.

## Experimental equipment

The equipment (Figure 2) was designed to study flow as well as heat transfer from impinging slot jets, with capability of providing throughflow at the impingement surface, a variable known to enhance transport phenomena at the surface considerably. Here only those features of the equipment[11] that are relevant to the flow and heat transfer measurements (without throughflow) are mentioned.

Air passed from the main blower discharge silencer through a flanged aluminum header of 200-mm diameter. The header supplied air to three 100-mm OD, 160-mm long aluminum pipes, welded to the header at a spacing between centerlines of 160 mm. Each of these pipes contained a manually operated butterfly valve for control of flow rate to each plenum chamber. These rectangular Plexiglas plenum chambers (250 mm deep and 100 × 250 mm in cross section) adapted the flow from the 100-mm circular inlet to the 250-mm slot nozzle entrance. Air entering the well-aligned plenum chambers passed through a layer of aluminum honeycomb to straighten the flow, then through two 100 mesh screens spaced 50 mm apart to dampen turbulence. The slot nozzle plate was likewise spaced 50 mm below the second screen. The plenum-to-nozzle contraction ratio was sufficiently large (in the range of 7:1–40:1) so that, combined with the screens, conditions at the nozzle exit were a flow with well-dampened turbulence and a uniform velocity profile in the spanwise direction of the jet.

Aluminum nozzles in five configurations enabled study of effect of the ratio, nozzle area/impingement surface area, termed the percent open area, from $f = 1.56$ percent to $f = 8.313$ percent. While using one set of plenum chambers and hence a fixed spacing (160 mm) between adjacent slot jets,

five values of percent open area, $f$, were obtained with a single test section by using five sets of nozzle plates of varying nozzle width, $w$. The nozzles were machined according to the American Society of Mechanical Engineers Standard[12] for short, elliptic entry, round nozzles, using hydraulic diameter in place of pipe diameter. The five sets of 250 mm long geometrically similar nozzles were 2.5, 3.3, 5.0, 10.0, and 13.3 mm wide. The high values of nozzle aspect ratio varied from 100:1–18.75:1 and assured two-dimensionality of flow at the nozzle exit.

A key feature of this experimental design was that impingement flow was exhausted through ports located between neighboring jets (Figure 1). Thus, symmetrical flow without cross flow of air after impingement was achieved. The two Plexiglas retaining walls prevented the jets from spreading in the traverse direction, thereby maintaining their 2-D character. The width of the rectangular exhaust ports between the jets were at most cases four times the nozzle width ($4w$) in order to minimize pressure loss through the exit. The exit ports at each end were half the width of the interior ones as they accommodated only half the flow of other ports. For each test case a fine adjustment on the position of each end wall was used to achieve this flow specification. Furthermore, static pressure measurements on the impingement plate were used to control the uniformity and similarity of the three inlet jets. The end walls were provided with a variable area slit that allowed hot wire traversing of the jet flow system.

A basic question in the use of such a test model is whether it actually represents a similar multiple jet system with a large number of jets, as would be found in an industrial application. An extensive set of impingement surface pressure profiles established that the flow within each inlet nozzle-exhaust port flow cell was completely symmetrical over the central two thirds of the test unit, i.e., from the centerline of one of the outer jets, through the central jet, to the centerline of the other outer jet. Thus, as the evidence was that two jets might have been sufficient, the use of a three-jet system provided a reliable replication of multiple confined slot jet systems of a large number of jets. The single jet system was obtained by removing the nozzle blocks for the two outside jets, hence the confinement surface comprised the two central jet nozzle blocks.

### *Velocity and turbulence measurements*

Turbulence measurements were made using the following DISA 55M System: a constant temperature anemometer (DISA 55M01), an electronic linearizer (DISA 55D35), and a Tektronix 466 dual-beam storage scope. The probe was mounted on a (DISA 55H21) probe holder, which was in turn screwed concentrically to a 20-mm diameter tube (probe support), entering the test section from the 250-mm end wall. The probe was mounted on a manual traversing mechanism (United Sensor and Control Corporation, Watertown, MA, USA), with Vernier-type graduations, in increments of 0.5 mm. Both Vernier and protractor were friction loaded with adjustable springs and balls for easy accurate rotation to any angle. The unit was mounted on a heavy tripod, which, as it was designed for high-speed photography, was sufficiently robust to minimize probe vibration.

A standard (DISA 55P04 and 55P14) right angle, single-wire probe was used to measure axial mean velocity ($U$) and fluctuating velocity ($u'$) along the jet centerline and downstream of the nozzle exit. The gold-plated hot wire probes, 1.2 mm long and 5 $\mu$m in diameter, caused minimal disturbance to the flow around the sensitive part of the wire. Integration times for the mean voltages were 10 seconds, while the rms voltmeter was set at a time constant of 3 seconds. Standard procedures were followed to obtain the linearized signal from the single wire probe.

The probe was calibrated in situ on the jet axis at 1 mm from the exit plane of the ASME nozzle, which generated a flat mean velocity profile and low turbulence level. This calibration was done on the basis of Pitot tube measurements at corresponding values of jet flow rate. The calibration of each hot wire probe was verified after each test run.

### *Static pressure measurements*

Static pressures were measured with 1-mm OD stainless steel tube (0.76 mm ID) pressure taps spaced 5 mm apart in the streamwise direction along the midspan centerline of Plexiglas impingement surface. At one streamwise location, close to the midpoint of the impingement surface, 10 static taps were located in the spanwise direction, i.e., along a line at 90° to the other 38 taps. The spanwise pressure profile was obtained at various streamwise locations by horizontal traversing of the plate. The pressure from the static taps through tygon tube was measured by two Statham unbonded strain gauge differential pressure transducers (range, 0–6.9 and 0–1.1 kN/m$^2$). Both units were equipped with calibrated zeroing bridge. A Data Precision Inc., Model 3400 digital voltmeter was used to read this pressure transducer. A 48-port scanivalve facilitated switching between the static pressure taps. Uncertainty in static pressure measurements at the impingement surface was at most 3 percent.

### *Heat flux measurements*

The impingement plate was heated by 12 independently controlled electrical heaters, each being a single length of 24 AWG (0.5 mm diameter) Inconel wire, electrically insulated with a magnesium oxide layer, then shielded with a stainless steel sheath (1.0 mm OD). Maximum temperature variation across the lateral and traverse width of heat transfer surface of the sensor was found to be less than 0.1°C, thus ensuring a very close approach to constant temperature boundary condition. For the present experiments the heat loss from the lower surface of the sensor was minimized by mounting a 250 × 100 × 10 mm sheet of Marinite-36 asbestos cement to cover the heat flux sensor and the adjacent plate.

The heat flux meter comprised the 13th separately heated section of the porous bronze impingement surface (size, 10 × 760 × 250 mm; surface finish, 1.25–5.00 $\mu$m [rms]), but differed from the other 12 heated sections in that it was thermally insulated from the surrounding plate. It was instrumented so that the electric power dissipated by heat transfer from it could be measured precisely.

The heating circuit (Figure 3) consisted of an Inconel heating wire ($R_h = 0.6$) embedded in the heat flux sensor and a precision resistance ($R_P = 0.1$). A variable DC power supply, Lamda LP-410A-FM (Manville, NY, USA), was manually adjusted to achieve the desired sensor surface temperature. The precision resistance, $R_P$, was used for calculation of the current, the voltage, $V_P$, being measured by a 5.5 digits multimeter, Model 3500 (Data Precision, Wakefield, MA, USA). The voltage drop, $V_h$, across the heating wire, $R_h$, was measured by a 3.5 digits multimeter, Model 175 (Data Precision). At steady state the local heat transfer coefficient is calculated as

$$h = Q_{conv}/A_s(T_s - T_j)$$

where

$$Q_{conv} = P_s - Q_{cond} - Q_{rad}$$

$$P_s = V_h(V_P/R_P) - (V_P/R_P)^2 R_{lw}$$

Heat losses at the lower surface of the sensor via conduction, $Q_{cond}$, and at the upper surface via radiation, $Q_{rad}$, were estimated

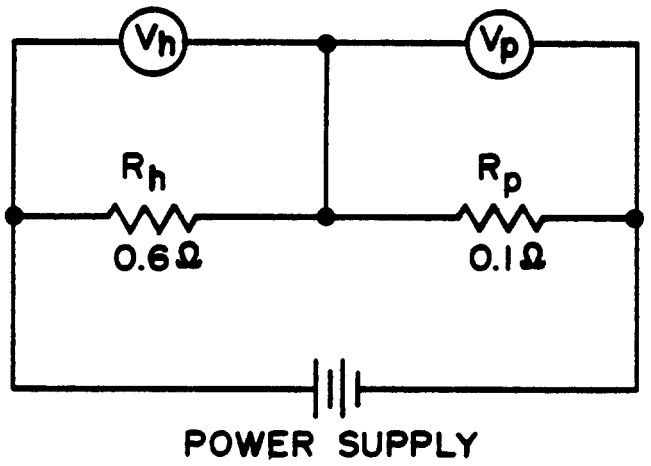


*Figure 3* Heating circuit for the heat flux sensor

following standard procedures. Radiation heat loss was negligible, less than 0.5 percent of the total heat transferred.

Local convective heat transfer, $h$, based on the temperature difference $T_s - T_j$, was normalized in the form of Nusselt number, $\mathrm{Nu} = hw/k$, with thermal conductivity evaluated at the nozzle exit temperature as was kinematic viscosity for Re. Uncertainty in heat transfer measurements was tested at two conditions, i.e., high and low heat transfer, and found to be 2.5 percent and 30 percent, respectively. Reproducibility of the results was better than 4 percent.

The width of the sensor, 3.7 mm, was determined critically by solving the 2-D heat conduction partial differential equation numerically as two conflicting requirements had to be considered: (1) minimization of the averaging effect of the sensor size and (2) minimization of the blockage effect of electric heating wire of the cross-sectional area of porous bronze sensor. The second requirement was important for the heat transfer measurements made under normal throughflow conditions, which are not reported here.

Obtaining a complete heat transfer rate profile in the direction crosswise to the fixed position nozzle slots was achieved by horizontal traversing of the impingement surface, with its single heat flux sensor over a lateral distance of 320 mm. Traversing of the impingement surface was done by means of a 1/3 HP variable speed AC electric motor via a screw rod connecting one end of the impingement surface. The screw rod motion was controlled through the motor by means of a specially designed variable transformer with an on–off timer option. A stopping time of about 30 minutes was found to be sufficient at a particular position to ensure steady-state conditions of the heat flux sensor. The location of the sensor was read from scale attached to the side wall.

Variation in one of the fundamental parameters of this study, the impingement surface spacing from the jet nozzle ($H$), was achieved by providing a gear mechanism for adjusting the vertical position of the impingement surface suction box unit under a multiple jet nozzle assembly maintained at a fixed position. The impingement surface spacing was monitored by means of an accurate scaling on the retaining walls.

## Results and discussion: flow

### *Flow characteristics at the nozzle exit*

The nozzle geometry selection, i.e., ASME standard elliptic entry shape, was made with the objective of having for all cases a uniform boundary condition for the inlet jet, i.e., flat velocity profile and low uniform turbulence across the jet at the nozzle exit. Measurement of profiles of axial mean and fluctuating velocity, $U$ and $u'$, across nozzle width for all five values of $w$ established that this objective was achieved, i.e., the profiles of mean and turbulent velocity were uniform over the central 90 percent of the nozzle width. Turbulence intensity in the central region across the nozzle was less than 1 percent due to strong acceleration of the flow, rising to the normal peak near the nozzle walls. Over the range $10{,}800 < \mathrm{Re} < 18{,}700$, however, this level increased in a small but consistent way from 0.65 percent for the two narrowest nozzles, successively to 0.7, 0.75, and 0.8 percent as $w$ increased to 5, 10, and 13.3 mm. As a fixed plenum chamber width was used throughout, the area contraction ratio decreased as nozzle width increased. Thus, the higher nozzle exit turbulence intensity for wider nozzles is a result of correspondingly less contraction and hence less suppression of turbulence from the flow entering the nozzle. No effect of jet Reynolds number on turbulence intensity over the same range was observed.

### *Flow field downstream from the nozzle exit*

Development of a single free jet and multiple jets was studied at the middle jet position for a typical value of jet Reynolds number, $\mathrm{Re} = 11{,}000$, for all five values of $w$. For the study of single free jet development up to $18w$ from the nozzle exit, the impingement surface was located sufficiently far, at $30w$, so that no influence from the impingement surface existed over the region studied.

**Single jet.** Immediately downstream of the nozzle exit the turbulence in the free jet increases extremely rapidly due to high degree of mixing generated in the region under the nozzle walls. Thus, lateral profiles of fluctuating velocity peak at around $x/w = 0.5$ near the nozzle exit. By only one nozzle width downstream of nozzle exit the fluctuating velocity at $x/w = 0.5$ reaches a peak value of about 25 percent of the jet exit velocity from a level of lower than 1 percent at the nozzle. By about $16w$ downstream the location of these peaks in $u'$ moves outward to about $x/w = 0.75$ due to the general outward expansion of the developing jet. By contrast, lateral profiles of axial turbulence intensity do not peak but, because of the decrease of axial mean velocity in the lateral direction, continue to increase with lateral distance out to about $x/w = 1.5$, i.e., as far as accurate measurements could be made. Graphical presentation of $u'$ and turbulence intensity profiles can be found elsewhere.[11]

Along the jet centerline the turbulence fluctuating velocity peaks at about $8w$ downstream (Figure 4). However, by $18w$ downstream the continuously increasing turbulence intensity ($u'/U_0$) reaches about 20 percent. For a slot jet the axial fluctuating velocity along the jet centerline is unaffected by the impingement surface up to $1w$ from surface, the closest that was measured in the present study. On the other hand axial turbulence intensity along the jet centerline begins to increase sharply at about $4w$ from the impingement surface when the spacing is $H/w = 19$ due to corresponding drop in axial mean velocity (Figure 5) that starts at around $0.2H$ from the impingement surface, with unchanged fluctuating velocity. These observations are in agreement with those by Obot[13] for a turbulent impinging round jet and by Gutmark *et al.*[14] for a turbulent impinging slot jet.

Despite high levels of turbulence present immediately downstream of the nozzle exit, small differences in turbulence intensity (0.65–0.85 percent) at the nozzle exit as a function of $w$ does show its effect on the flow development of jet after

discharge. These differences in turbulence intensity continue and grow in the free jet region and are easily detected along the jet centerline even at $18w$ from the nozzle exit (Figure 4). Hence the onset of decay of axial mean velocity on Figure 5 takes place earlier with the larger nozzles due to increased lateral transport of mean momentum as a consequence of higher levels of axial turbulence. The length of the potential core thus decreases from $4w$ at $w = 2.5$ mm to $3w$ at $w = 13.3$ mm. The small but consistent effect of nozzle width were likewise detected on related variables such as the locations of kinematic and geometric origins of the single free jet and jet half-width.[11]

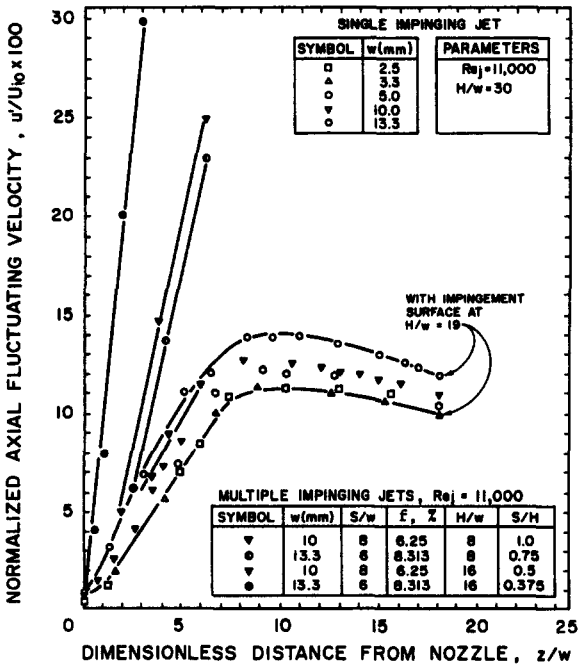


*Figure 4* Profiles of fluctuating velocity at the jet centerline

**Multiple jets.** A multiple slot jet system with exhaust ports alternating with inlet nozzles jets could be described as noninteracting when the internozzle spacing, $S$, is sufficiently wide. As in a noninteracting system jets can effectively be considered as an array of widely spaced single jets, single jet data can be used to predict transport phenomena in the impingement region. In a contrary case where the internozzle spacing is not wide enough so that the jets are interacting, special multiple jet data would be required to predict transport phenomena at the impingement region. It is important to have a criterion for distinguishing between these two types of systems. In this section this criterion will be sought by comparing centerline flow characteristics of a multiple jet system with those of a corresponding single jet.

Here it is proposed to view the multiple jet system with symmetrical exhaust ports as an assembly of repeated flowcells, a flowcell being defined as the volume contained by the impingement and confinement surfaces and the centerlines of adjacent inlet nozzles and exhaust ports. As the lateral and axial length of such a flow cell is, respectively, $S$ and $H$, the ratio $S/H$ emerges as one of the nondimensional geometric parameters to characterize a flow cell. As there is a third dimension involved, i.e., nozzle width, $w$, complete similarity between flow cells would require equality of two nondimensional ratios of the three dimensions involved, $S$, $H$, and $w$. Thus, in addition to $S/H$, another independent nondimensional ratio, either $S/w$ (or $f = w/2S$) or $H/w$ is required for considerations of geometric similarity. Importance of the parameter $S/H$ to characterize the flow field of a multiple jet system will be clearer in subsequent discussions.

Effect of multiple jets on jet centerline flow conditions was studied at four flow cell proportions ranging from $S/H = 0.375$ to $S/H = 1$. These four values of $S/H$ were obtained by appropriately combining two values of nondimensional nozzle-to-surface spacing, $H/w = 8$ and 16, with two values of nondimensional nozzle-to-exhaust centerline spacing, $S/w = 8$ and 6.

Figures 4 and 5 document the dependence on geometric parameters, particularly on $S/H$, of axial fluctuating velocity and axial mean velocity along the jet centerline. With respect to profiles of fluctuating velocity (Figure 4) for the highest flow

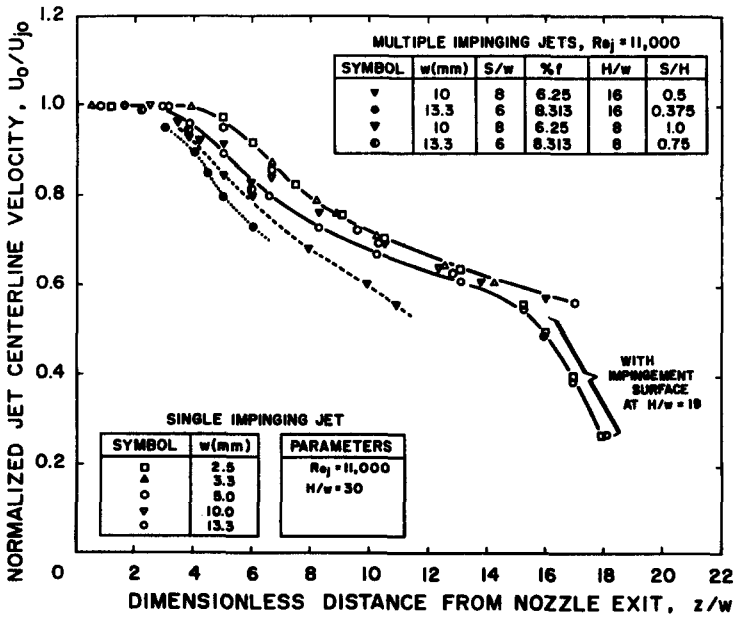


*Figure 5* Profiles of mean velocity at the jet centerline

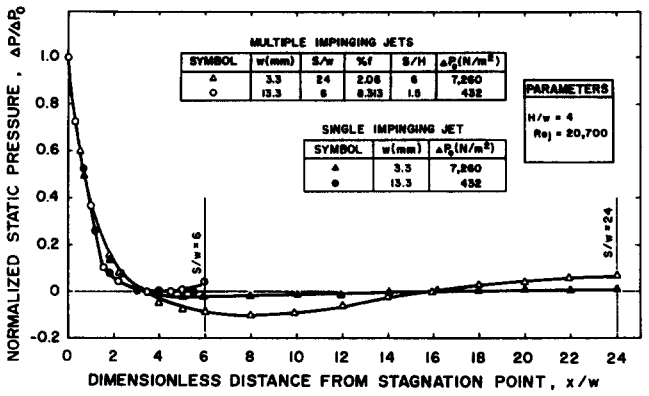


*Figure 6* Lateral profiles of static pressure at the impingement surface for single and multiple slot jets at $H/w = 4$

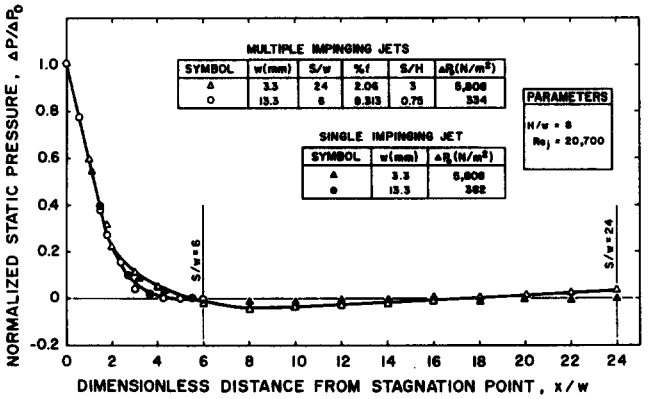


*Figure 7* Lateral profiles of static pressure at the impingement surface for single and multiple slot jets at $H/w = 8$

cell ratio, $S/H = 1$, there is a marginal difference, $<15$ percent, between a single and a multiple jet system in the whole range of measurements made for this $S/H$ ratio, i.e., $0 < z/w < 6$. For the narrower flow cell, $S/H = 0.75$, Figure 4 indicates that up to about $z/w = 2.5$ the single and multiple jet centerline $u'$ profiles are indistinguishable. Beyond this $z/w$ value the strong interaction between multiple jets is apparent from the rapidly increasing centerline $u'$. For the next narrower cell, $S/H = 0.5$, Figure 4 indicates interaction reaches the centerline at about $z/w = 2$. For the narrowest cell, $S/H = 0.375$, the multiple jets are so strongly interacting there is no discernible $z/w$ value before the centerline $u'$ profile displays a penetrating interaction. By only $z/w = 0.5$ the centerline fluctuating velocity for the $S/H = 0.375$ flow cell is double that for the equivalent single jet and by $z/w = 3$ it is four times as high. Essentially the same trend is observed if mean velocity (Figure 5) is taken as the criterion to characterize the onset of the extent of interaction at the jet centerline, i.e., effectively no interaction at $S/H = 1$ and strong interaction at $S/H = 0.375$. The exact value of the critical $S/H$ ratio where the effect of jet-to-jet interaction starts to show a penetrating effect on the jet centerline profiles cannot be defined from the present centerline profiles, but should be some value in the narrow range $0.75 < S/H < 1$. The question of the extent of interaction between jets will be reiterated in the following sections, with respect to the flow field and heat transfer at the impingement surface.

### *Flow field at the impingement surface*

Flow at the impingement surface is analyzed through examination of static pressure profiles for a wide spectrum of flow cell geometry, $0.375 < S/H < 6$, and over the entire range of jet Reynolds number, $5000 < \mathrm{Re} < 43{,}800$. As the pressure profiles in the central flow cells were practically identical, in the following presentation of the results only one representative pressure profile is used for the multiple impinging jets.

**Single jet.** Static pressure profiles obtained for a single jet with $w = 3.3$ mm and 13.3 mm, and $H/w = 4$, 8, and 16, at $\mathrm{Re} = 20{,}700$, over a length $S = 80$ mm are displayed in Figures 6–8, along with the multiple jet data. They typically decrease from a maximum at the stagnation point to nearly ambient pressure by $3$–$8w$ from stagnation, the latter location naturally increasing in the increasing $H/w$. Downstream from $x/w = 3$–$8$ the developing wall jet is a region of flow deceleration where the static pressure increases slightly up to $x/w = 14$, thereafter remaining steady.

**Multiple jets.** Static pressure profiles were measured for the six limiting combinations of flow cells, $S/H = 6$, 3, and 1.5 for $S/w = 24$ at $H/w = 4$, 8, and 16, and $S/H = 1.5$, 0.75, and 0.375 for $S/w = 6$ at $H/w = 4$, 8, and 16.

For the widest flow cell, $S/H = 6$, there occurs first the usual impingement region, then a particularly long wall jet region, and a region around the centerline of the exit ports, which is unique to the exhaust flow arrangement used for the first time in this study and will be named the exit port flow region. Here the wall jet type flow is succeeded by a flow from the impingement surface to the exhaust port in the confinement surface. Thus, lateral velocities in this region are approaching zero, the limiting value at the exit port centerline, while the normal velocity away from the impingement surface is becoming correspondingly large. In any case, for a multiple jet system with large internozzle spacings it may be expected that conditions at the impingement surface could be well predicted from data for a single jet for the same flow and geometric parameters.

At the other extreme in flow cell proportions, i.e., for the narrowest flow cell, $S/H = 0.375$, the wall jet region effectively vanishes, there being essentially a transition from an impingement flow directly to the exit port region flow. For flow cells of proportions as narrow as this it may be anticipated that extensive interaction would occur between inlet jets and adjacent exit flows, with the result that conditions at the impingement surface would be greatly different relative to the corresponding single jet.

For $\mathrm{Re} = 20{,}700$, each of Figures 6, 7, and 8 show impingement surface profiles for one value of nozzle-to-surface spacing, $H/w$. The absolute value of stagnation pressure, $\Delta P_0$, to which lateral profiles are normalized, are tabulated in each figure. Also shown in these figures are comparative data for a single slot jet. Multiple jet pressure profiles are nearly coincident with those for a single jet except for the narrowest flow cell, $S/H = 0.375$. In the latter case, the large value of impingement surface pressure at the exhaust port centerline, i.e., about 60 percent of the stagnation pressure, reflects the large dissipation of energy from the spentflow to the countercurrent inlet jet flow in a flow cell this narrow.

As pointed out earlier, as the width of the flow cell in a confined multiple slot jet system is decreased, the extent of the wall jet region decreases and finally disappears for a very narrow flow cell. At $\mathrm{Re} = 20{,}700$, it is evident from Figures 7 and 8 that this limit is reached for a narrow flow cell of proportions $S/H$ at some value between the limit $1.5 < S/H < 0.375$. The exact value of this limiting flow cell proportion would be the

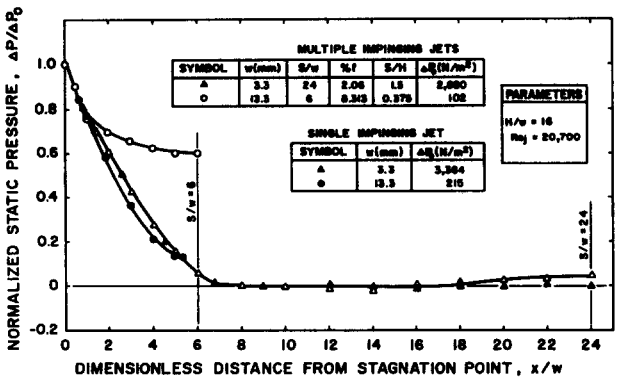


*Figure 8* Lateral profiles of static pressure at the impingement surface for single and multiple slot jets at $H/w = 16$

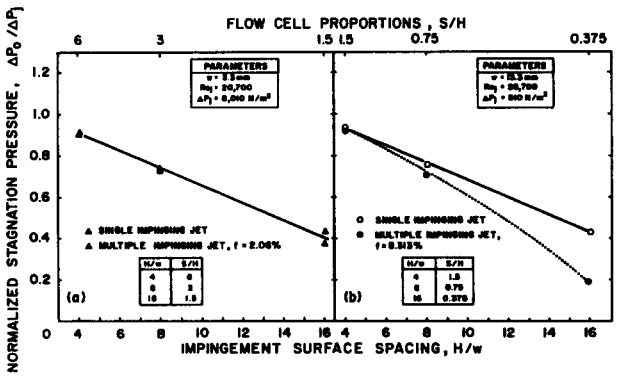


*Figure 9* Effect of impingement surface spacing on stagnation pressure for single and multiple slot jets

value of $S/H$ at which the impingement surface pressure profile for the multiple jet system just starts to deviate from that for a single jet.

Because static pressure in Figures 6–8 is normalized with respect to stagnation pressure, $\Delta P_0$, it is not clear when interaction between jets affects the stagnation pressure. Figure 9 displays stagnation pressure as a function of impingement surface spacing. For this figure $\Delta P_0$ is normalized with respect to the pressure difference across the nozzle, $\Delta P_j$. The data of both Figures 9a and 9b show no significant difference between multiple and single jet data for flow cells over the range $6 < S/H < 1$. From Figure 9b, however, it is observed that somewhere in the range $1 > S/H > 0.75$ the multiple jet system begins to drop below that for a single jet. The observation parallels the similar interrelation displayed for the free jet region on Figures 4 and 5.

Figures 6–8 indicate that $H/w$ remains a parameter for pressure profiles of single and noninteracting multiple slot jets. An alternate way of representing these profiles would be to normalize the lateral dimension of pressure profiles with $H$, which proved to be very useful as a normalizing parameter for $S$. This approach investigated through the use of $x/H$ as the lateral dimension on Figures 10 and 11. The data of these two figures, at Re = 20,700, relates to two greatly different nozzle spacings, $S/w = 24$ and 6, which, with a range of nozzle-to-surface spacing, $H/w = 4$, 8, and 16, corresponds to flow cells from very wide, $S/H = 6$, to very narrow, $S/H = 0.375$. As the jets in multiple jet system with a flow cell ratio as narrow as 0.375 are strongly interacting the impingement surface pressure profile for this $S/H$ ratio is quite different than the profiles for larger $S/H$ ratios as it was the case on Figure 8. On the other hand, for the five profiles for noninteracting jets, $6 > S/H > 0.75$, it is highly significant from Figures 10 and 11 that with lateral distance normalized with respect to $H$, the pressure profiles effectively collapse to a single profile in the stagnation flow region. Specifically all half pressure widths (where $\Delta P/\Delta P_0 = 0.5$) occur at around $x/H = 0.15 \pm 0.01$, and the location for $\Delta P/\Delta P_0 = 0.05$ is also about the same for all cases, i.e., at $x/H = 0.5 \pm 0.1$.

Although the profiles of normalized surface pressure relative to $x/H$ effectively collapse to a single profile over the impingement region, the extent of relatively flat region of pressure profile wherein the pressure approaches to that at the exhaust port varies considerably. The lateral extent of this flat region of the profiles ranges from about $5.5H$ for the case of the widest flow cell, $S/H = 6$, down to $0.25H$ for a relatively narrow flow cell, and $S/H = 0.75$, the narrowest flow cell in this series, which did not give the strongly interacting multiple jet behavior represented by $S/H = 0.375$. Only in this flat region of the pressure profiles there is a slightly more variation between the data for different values of $H/w$.

While $w$ is a satisfactory basis for normalizing lateral distance from stagnation point for some purposes, the above observations indicate that the maximum degree of similarity is

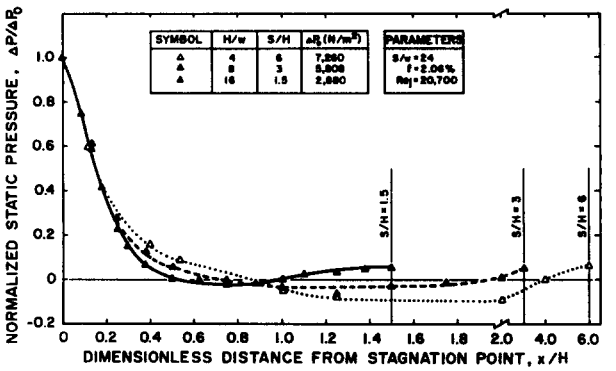


*Figure 10* Lateral profiles of static pressure at the impingement surface for multiple slot jets for $f = 2.06$ percent

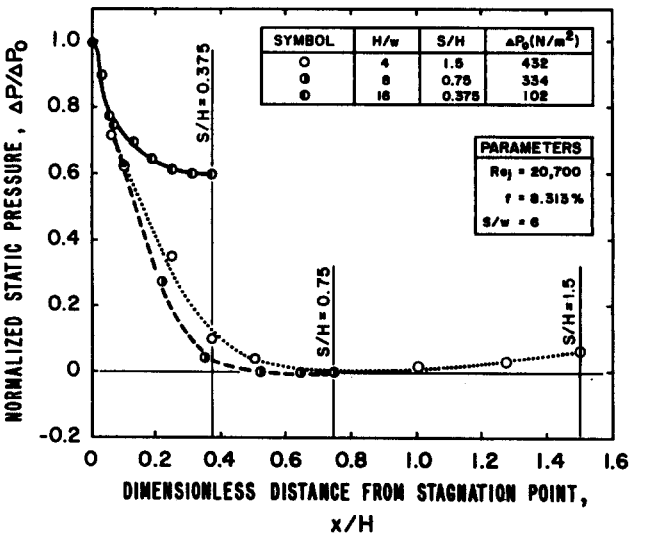


*Figure 11* Lateral profiles of static pressure at the impingement surface for multiple slot jets for $f = 8.31$ percent

obtained by lateral distance from stagnation point nondimensionalized with respect to impingement surface spacing $H$. The degree to which normalizing lateral distance with respect to $H$ yields a common pressure profile at Re = 20,700 provides further evidence supporting the concept that $S/H$ is a basic characteristic variable of general utility for confined multiple slot jet systems.

For noninteracting as well as for strongly interacting multiple jets, the normalized surface pressure profiles are remarkably independent of the jet Reynolds number over the wide range of Re tested.

In summary, two alternate flow criteria used to define the critical size of flow cell, $(S/H)$, which separates noninteracting from interacting multiple confined slot jet systems were the axial flow characteristics along the jet centerline of the free jet region, and pressure profiles at the impingement surface. For a given value of $S/H$ the degree of departure of the flow characteristics along the jet centerline and at the impingement surface relative to those for a single impinging jet indicates the extent of interaction in the multiple impinging jet system. Although the normalized pressure profiles for the multiple jet system are not measurably different from those of a single jet until $S/H$ is less than 0.75, the other criteria, i.e., axial flow field along the jet centerline, and reduction in stagnation pressure for multiple jet system relative to a single jet, indicate that the value of $(S/H)$ is between 0.75 and 1. As jet centerline turbulence and stagnation point pressure are the most sensitive criteria, it may therefore be concluded that $(S/H)_c$ is in the range 0.75 and 1.

## Results and discussion: heat transfer

Similar to pressure profiles, surface convective heat transfer in the central four flow cells of the six flow cell system (Figure 2) was shown to be symmetrical and indistinguishable.[11] Therefore, in the subsequent discussions only one representative heat transfer profile for each case is displayed.

### *Stagnation point heat transfer*

In the study of impingement transport characteristics the stagnation point assumes exceptional importance for its high rate of heat transfer. In order to increase the overall rate of heat transfer for a multiple impinging slot jet system the frequency of these stagnation maxima should be increased.

With jet-to-jet interaction the centerline mean velocity decays faster with a significant enhancement in the axial fluctuating velocity. As these two effects produce opposite trends in the transport phenomena near the surface, the resulting net effect on the stagnation point heat transfer cannot be predicted.

Although the present study is oriented to heat transfer under multiple confined jets, the experimental program included the corresponding single confined slot jet in order to provide a base case for analysis of the multiple jet configuration. The single impinging jet data indicated that $Nu_0$ passed through a maximum at around $H/w = 8$ as was reported by a number of previous studies.[3,6,8,15,16] The data also indicated an effect due to nozzle width, $w$. The first effect, i.e., the maximum around $H/w = 8$, is due to the effect of impingement surface spacing on $Nu_0$ through the corresponding effects of centerline mean velocity, $U_0$, and turbulence intensity approaching stagnation. After the end of the potential core region, which is about $3-4w$, $U_0$ decreases with the square root of distance from nozzle exit. In the mean time turbulence intensity $(u'/U_0)$ increases with distance from nozzle exit, an increase at first sharp, but leveling out after $8w$ from the nozzle exit. For spacings up to about $H/w = 8$ the effect on $Nu_0$ of the rapidly increasing turbulence intensity is more important than the opposing effect of decreasing $U_0$. Beyond $H/w = 8$ the relative importance of these two effects are reversed. Occurrence of maximum $Nu_0$ again at about $H/w = 8$ (Figures 12 and 13) independently of Re and $S/H$ indicates that varying relative importance of the opposing effects of $H/w$ on axial mean velocity and turbulence intensity continue to act in a similar way for a multiple jet system.

The second effect, i.e., the appearance of $w$ as a parameter in constant Reynolds number constant $H/w$, can be explained again with the corresponding effects of mean velocity and turbulence intensity on $Nu_0$. As reported previously turbulence intensity at the nozzle exit showed a small but consistent increase from 0.65 percent for the narrowest nozzle width, 3 mm, to 0.7, 0.75, and 0.8 percent as $w$ increased to 5, 10, and 13.3 mm. These small differences in nozzle exit turbulence intensity were shown to grow even to bigger differences with increasing distance from nozzle exit, e.g., at $H/w = 8$ the centerline turbulence intensity for the largest $w$ was about 25 percent higher than for the smallest $w$. The difference between the mean centerline velocities for these two $w$ values was small, only 3 percent less for $w = 13.3$ mm than for $w = 3$ mm. Through the combined effects of these two parameters the net expected enhancement of about 20 percent in Nu is compared with the observed difference of about 17 percent at $H/w = 8$. With increasing nozzle-to-surface spacing the effect of $w$ as a systematic parameter is significantly reduced if allowance is made for another contributing factor, i.e., the averaging effect of the sensor due to its finite size. This was estimated to be around 4 percent for the smallest $w$, 3 mm, and comparatively less for larger nozzle widths.

The criteria of interacting/noninteracting multiple jet system is investigated by examining the corresponding values of $Nu_0$ in Figures 12 and 13 presented, respectively, for a relatively low, $f = 2.06$ percent, and for the highest open area, $f = 8.313$ percent used in the experiments. The results for the

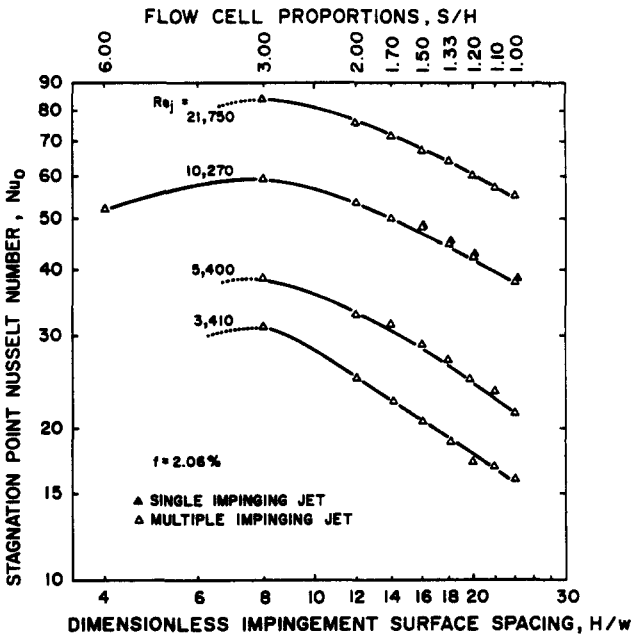


*Figure 12* Effect of impingement surface spacing on $Nu_0$ for multiple jet system ($f = 2.06$ percent) and for a single jet ($w = 3.3$ mm)

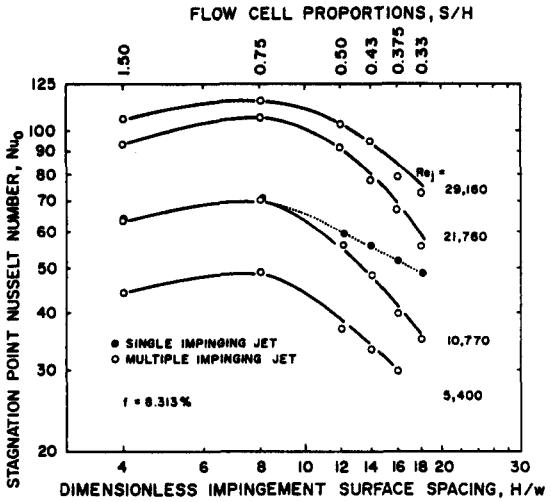


*Figure 13* Effect of impingement surface spacing on $Nu_0$ for multiple jet system ($f = 8.313$ percent) and for a single jet ($w = 13.3$ mm)

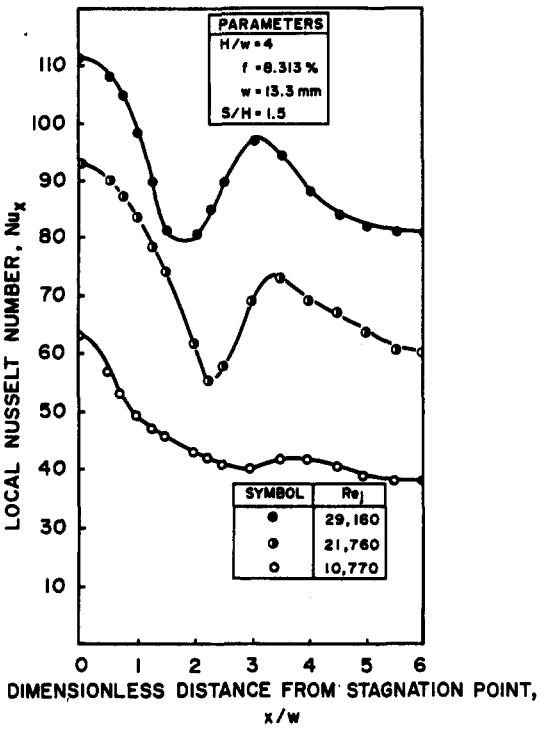


*Figure 14* Effect of jet Reynolds number on lateral profiles of Nu for $H/w = 4$

other three values of $f$, i.e., 1.56, 3.125, and 6.25 percent, are not included here due to limited space, but essentially show the same features.[11]

For $f = 2.06$ percent (Figure 12) the data for both single and multiple impinging jets coincide down to the lower limit of $S/H$, i.e., $S/H = 1$, thus indicating that for this $S/H$ the multiple jets are still noninteracting at the stagnation point. For $f = 8.313$ percent, Figure 13 shows, however, that the multiple jet $Nu_0$ starts to drop below that for a single jet after approximately $S/H = 0.7$, with the deviation at smaller values of $S/H$ increasing such that by $S/H = 0.33$ the multiple jet Nu is about 27 percent lower. The reduction of $Nu_0$ for the multiple jet system at low values of $S/H$ is an indication of the interaction between jets having reached the inlet jet centerline. Although single jet results were obtained at only Re = 10,500, from the similarity of slope of curves on Figures 12 and 13 it appears that, as $S/H$ decreased, the effect of multiple jet interaction begins at about $S/H = 0.7$ over a range of Re.

## *Lateral profiles of heat transfer*

Figures 14–16 provide typical profiles of Nu for the nozzle-to-surface spacings, $H/w$, of 4, 8, and 24 over a range of Re. For the flow cell proportions as wide as those of Figures 14–16, i.e., $S/H > 1$, jet-to-jet interaction does not yet affect the profiles as can be detected from the excellent agreement between the single and multiple jet data presented in Figures 15 and 16 for the Re = 11,000 profiles. By deferring the discussion about the effect of $S/H$ on Nu profiles attention is given here to the general features of these profiles.

The principal features of the profiles for $H/w = 4$ (Figure 14) are the occurrence in each case of an off-stagnation maximum and intervening minimum. The minimum has been identified by previous investigators[3,6,8,15,16] as the beginning of transition from a laminar boundary layer present in the stagnation region to a turbulent one. This transition is

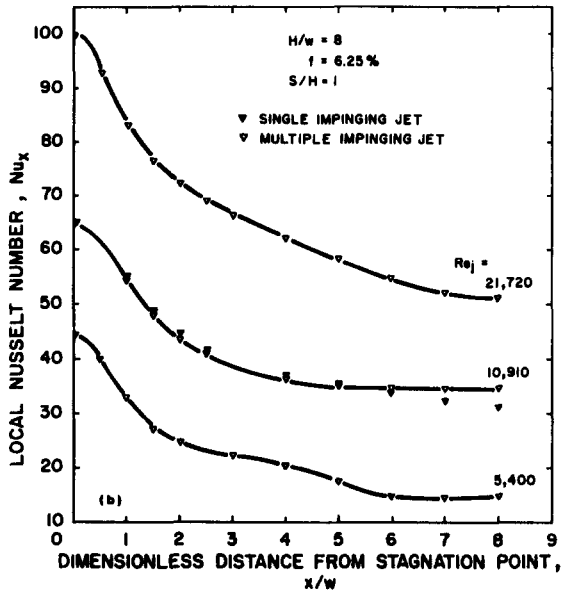


*Figure 15* Effect of jet Reynolds number on lateral profiles of Nu for $H/w = 8$

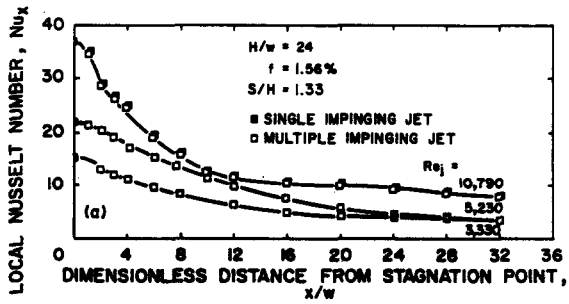


*Figure 16* Effect of jet Reynolds number on lateral profiles of Nu for $H/w = 24$ ($f = 1.56$ percent)

considered complete at the location of the off-stagnation maximum. The decline in Nu beyond the off-stagnation maximum simply reflects increasing thickness of the turbulent boundary layer similar to the decline in Nu beyond stagnation maximum due to increasing thickness of the laminar boundary layer.

The lateral gradient of pressure at the impingement surface is considered to play a key role in boundary-layer transition from laminar to turbulent. As strongly negative pressure gradients in the stagnation region stabilizes the laminar boundary layer, an approximation is that transition occurs where the steep pressure gradient ends. For noninteracting multiple jet systems, i.e., for $S/H > 0.75$, it was established previously that the profiles of static pressure at the impingement surface display similarity when presented as a function of $x/H$. For these similarity profiles the stagnation region, defined as the location where static pressure drops to 5 percent of the stagnation pressure, was found to extend laterally a distance equal to half the spacing $H$. Application of these similarity findings for Nu profiles at $H/w = 4$ would then imply that the transition point would be near $x/w = 2$. In Figure 14 the Nu profiles in the range $10{,}700 < \mathrm{Re} < 29{,}000$ for $H/w = 4$ indeed display the minimum at $x/w = 2$, providing further support for this concept of transition.

As boundary-layer transition from laminar to turbulent is driven by the interaction between the surface and an impingement flow, which is highly turbulent, the finding that this transition occurs over a shorter distance from stagnation as Re increases is expected (Figure 14). Increased sharpness of the maxima and minima peaks in Nu profile with increasing Re at this short nozzle spacing is due to increased lateral static pressure gradient in the impingement region.

Further support of the hypothesis that the boundary layer is laminar at stagnation and goes through transition to become turbulent at the off-stagnation peak comes from the Reynolds number dependence of Nu at these two locations, i.e., the stagnation and off-stagnation maxima. In this respect, while the value of the exponent of Re term for the stagnation point, 0.57, is in close agreement with the 0.5 value associated with a laminar boundary layer, this dependence at the secondary maxima is found to be close to the 0.8 exponent associated with a turbulent layer.

In contrast to the profiles of Figure 14 for $H/w = 4$, the off-stagnation maxima and minima completely disappear at spacings larger than $H/w = 4$ (Figures 15 and 16). Two effects both act in the direction of elimination of these features of profiles at small impingement surface spacings. First, at larger distances from the nozzle exit the flow approaching the impingement surface is very turbulent. Second, at larger distances from the nozzle exit the stagnation pressure is significantly reduced. Thus, for $H/w = 8$ and 24 there is a considerable reduction in the lateral gradient in impingement surface pressure, identified earlier as the source of significant stabilizing effect to maintain a laminar boundary layer until the end of the stagnation region for $H/w = 4$.

### *Differentiation of multiple from single jets by the criterion of flow cell proportions,* S/H

The significance of the dimensionless geometric parameter $S/H$ was established previously. Here this parameter was found relevant for quantifying the geometric limit over which stagnation point heat transfer, $\mathrm{Nu}_0$, of multiple jets remains unchanged relative to the equivalent single slot jet. When entire Nu profiles are examined it is seen that the same $S/H$ ratio emerges as the relevant parameter.

At sufficiently high values of $S/H$ (Figure 16), the Nu profile for a multiple jet over the entire region from $\mathrm{Nu}_0$ to Nusselt number at the exit port centerline, $\mathrm{Nu}_e$, is coincident with that for the corresponding single jet. At an intermediate value of $S/H$ (Figure 15) the multiple jet profile of Nu and the profile for the equivalent single jet are to be coincident for some distance out from the nozzle centerline, after which Nu for the multiple jet becomes greater than for the single jet. At still lower values of $S/H$ (Figure 17), both types of deviations are found, i.e., a multiple jet system with $\mathrm{Nu}_0$ lower but $\mathrm{Nu}_e$ higher than for the corresponding single jet, so that such profiles cross at some point between the nozzle and exit port centerlines.

The behavior noted previously is displayed concisely in Figure 18, which summarizes all experimental evidence available for viewing the heat transfer performance of confined multiple slot jet systems relative to equivalent single jets. Thus, for $S/H > 1.5$, multiple slot jet systems may be simply viewed as an assembly of single jets. The value of Nu from nozzle centerline to exit port centerline is coincident with that for the corresponding single jet. When the dimensionless width of flow cell, $S/H$, becomes less than 1.5, heat transfer for the multiple jet system is enhanced under the exit port and for some distance toward the nozzle centerline while heat transfer at the nozzle centerline remains the same as for a single jet. When the dimensionless spacing between nozzles is reduced below $S/H = 0.7$, interaction between the closely spaced counter-current flows of inlet jet and exhaust streams penetrates to the nozzle centerline where it is reflected in reduction of Nu for multiple jets relative to an equivalent single jet. Nu for multiple jets is seen to decrease very sharply as $S/H$ reduced below the lower critical value of 0.7. As $S/H$ is reduced sufficiently, $\mathrm{Nu}_e$ also would eventually start to decrease. Although no matched sets of data for single and multiple jets in the present study were at a sufficiently low value of $S/H$ to show this effect, this expectation is reflected in Figure 18 through indication of an eventual downturn in Nu for some flow cell width less than the lowest experimental value, $S/H = 0.33$.

The flow analysis, based on comparison of stagnation point pressure and centerline turbulence characteristics, led to a $(S/H)_c$ value in the range 0.75–1. The heat transfer analysis indicated two critical values of $S/H$, i.e., $(S/H)_{ce} = 1.5$ and $(S/H)_{co} = 0.7$ for deviation of $\mathrm{Nu}_e$ and $\mathrm{Nu}_0$, respectively. The critical value $(S/H)_{co} = 0.7$ is in good agreement with the lower bound of the region, $S/H = 0.7$, suggested by the flow analysis. Considering the importance of heat transfer data for design of industrial equipment, conservatively, the earlier indication of jet-to-jet interaction at $S/H = (S/H)_{ce}$, should be used to differentiate an interacting system from that of a noninteracting one. Therefore, for a system with $S/H < (S/H)_{ce}$, specific

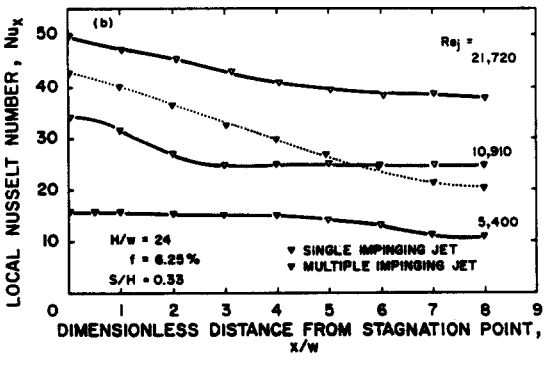


*Figure 17* Effect of jet Reynolds number on lateral profiles of Nu for $H/w = 24$ ($f = 6.25$ percent)

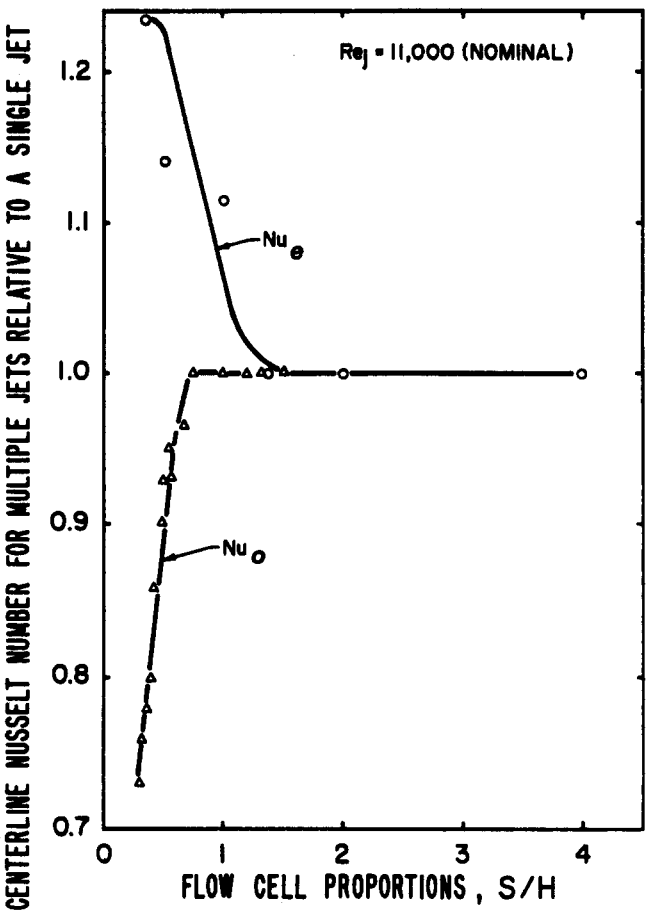


*Figure 18* Effect of flow cell proportion on centerline Nusselt number for multiple jets relative to a single jet

multiple jet data as is provided by the present study should be used.

## Conclusions

For multiple slot jets, a central question relates to the degree of interaction between inlet jet flows and intervening exhaust port flows, as evidenced by the corresponding effects on impingement surface heat transfer. To define the relationship between multiple jet systems and single jets, turbulence, mean flow, and heat transfer characteristics of both were obtained for comparable flow and geometric parameters.

The concept of flow cell, defined as the volume contained by the impingement and confinement surfaces and the centerlines of adjacent inlet nozzles and exhaust ports, to analyze a confined multiple impinging slot jet system with symmetrical exit ports in the confinement surface is introduced here for the first time.

It is shown through the analysis of profiles of pressure at the impingement surface that a flow cell is characterized effectively with a single nondimensional ratio $S/H$, the ratio of the lateral and axial length of flow cell, in the important impingement region. However, as a third dimension is involved, $w$, complete geometric similarity of flow cells would require to define another nondimensional ratio, either $S/w$ or $H/w$. Here it was shown that the second nondimensional ratio, with $H/w$ being the preferred one, was affecting the pressure profiles to some extent only in the region extending from the end of stagnation region to the exit port region.

The single jet data indicated that, for the elliptically contoured nozzles used in the present study, $Nu_0$ passed through a maximum at around $H/w = 8$ due to opposing effects of $H/w$ on $U_0$ and axial turbulence intensity. Occurrence of maximum $Nu_0$ again at about $H/w = 8$ independently of Re and $S/H$ indicates that $H/w$ effects are similar for a multiple jet system.

Results of analysis of the profiles of fluctuating and mean velocities at the jet centerline and stagnation point pressure for multiple and single impinging slot jets show that the critical $S/H$ ratio that separates noninteracting multiple impinging slot jets from interacting ones is between 1 and 0.75. On the other hand, at values of the ratio $S/H$ above an upper critical limit, $(S/H)_{ce} = 1.5$, Nu profiles for multiple jet over the entire region from $Nu_0$ to $Nu_e$ were coincident with those for the corresponding single jet. At an intermediate value of $S/H$ slightly below this critical value, the multiple jet profiles of Nu and the profile for the equivalent single jet were found to be coincident for some distance out from the nozzle centerline, after which Nu for the multiple jet is greater than for a single jet. At values of $S/H$ below a lower critical limit, $(S/H)_{co} = 0.7$, two types of deviations were found, i.e., a multiple jet system has a lower $Nu_0$ but a higher $Nu_e$ than for the corresponding single jet. It is evident that for design of multiple slot jet systems with $S/H < 1.5$, special multiple jet data should be used.

## References


1 Ahmad, I. Simulation of turbulent flow and heat transfer under an impinging round jet discharging into a crossflow. M.Eng. thesis, McGill University, Montreal, Canada, 1987

2 Saad, N. R., Mujumdar, A. S., Abdel Messeh, W. and Douglas, W. J. M. Local heat transfer characteristics for staggered arrays of circular impinging jets with cross-flow of spent air. *ASME Paper* 80-HT-20, 1980

3 Gardon, R. and Akfirat, J. C. Heat transfer characteristics of impinging two-dimensional air jets. *J. Heat Transfer*, 1966, **88**, 101–108

4 Schuh, H. and Pettersson, R. Heat transfer by arrays of two-dimensional jets directed normal to surfaces including the effects of a superposed wall-parallel flow. *Proc. 3rd Int. Heat Transfer Conf.*, Chicago, IL, USA, August 7–12, 1966, II, 280–291

5 Martin, H. Heat and mass transfer between impinging gas jets and solid surfaces. *Advances in Heat Transfer*. Academic Press, New York, 1977, 1–60

6 Cadek, F. F. A fundamental investigation of jet impingement heat transfer. Ph.D. thesis, University of Cincinnati, OH, USA, 1968

7 Gardon, R. and Akfirat, J. C. The role of turbulence in determining the heat transfer characteristics of impinging jets. *Int. J. Heat Mass Transfer*, 1965, **8**, 1261–1272

8 Kumada, M. and Mabuchi, I. Studies on the heat transfer of impinging jets. *Bull. JSME*, 1970, **13**, 77–85

9 Schauer, J. J. and Eustis, R. H. The flow development and heat transfer characteristics of plane turbulent impinging jets. Technical Report 3, 1963, Dept. of Mechanical Eng., Stanford University

10 Romanenko, P. N. and Davidzon, M. I. Heat transfer in the zone of accelerated flow during the normal impingement of a system of two-dimensional jets onto a flat surface. *Int. Chem. Eng.*, 1970, **10**, 223–228

11 Saad, N. R. Flow and heat transfer for multiple turbulent impinging slot jets. Ph.D. thesis, McGill University, Montreal, Canada, 1981

12 ASME Research report on fluid meters. *ASME*, 1971, New York, NY
13 Obot, N. T. Flow and heat transfer for round turbulent jets impinging of permeable and impermeable surfaces. Ph.D. thesis, McGill University, Montreal, Canada, 1981
14 Gutmark, E., Wolfshtein, M. and Wygnanski, I. The plane turbulent impinging jet. *J. Fluid Mech.* 1978, **88**, 737–756
15 Korger, M. and Krizek, F. Mass transfer coefficient in impingement flow from slotted nozzles. *Int. J. Heat Mass Transfer*, 1966, **9**, 337–344
16 Schlünder, E. U., Krotzsch, P. and Hennecke, W. Gesetzmabigkeiten der Warme-und Stofftbertragung bei der Prallstromung aus Rund-und Schlitzdtsen. *Chemie-Ing.-Techn.*, 1970, **42**, 333–338
17 Beltaos, S. and Rajaratnam, N. Plane turbulent impinging jets. *J. Hydraulic Res.*, 1973, **11**, 30–59
18 Martin, H. and Schlünder, E. U. Optimierung von Schlitzdtsentrocknern auf Grund neuer Versuchsergebnisse uber den Warme-und Stofftbergang in solchen Apparaten. *Chemie-Ing.-Techn.*, 1973, **45**, Jahrg, 290